Atmos. Meas. Tech., 10, 1–14, 2017
www.atmos-meas-tech.net/10/1/2017/
doi:10.5194/amt-10-1-2017
© Author(s) 2017. CC Attribution 3.0 License.

Atmospheric Measurement Techniques
Open Access
EGU

Remote sensing of volcanic CO_2, HF, HCl, SO_2, and BrO in the downwind plume of Mt. Etna

André Butz[1,5,6], Anna Solvejg Dinger[2], Nicole Bobrowski[2,3], Julian Kostinek[1], Lukas Fieber[2], Constanze Fischerkeller[1], Giovanni Bruno Giuffrida[4], Frank Hase[1], Friedrich Klappenbach[1], Jonas Kuhn[2], Peter Lübcke[2], Lukas Tirpitz[2], and Qiansi Tu[1]

[1]IMK-ASF, Karlsruhe Institute of Technology (KIT), Leopoldshafen, Germany
[2]Institute for Environmental Physics, Heidelberg University, Germany
[3]Institute of Geosciences, Johannes Gutenberg University Mainz, Germany
[4]Istituto Nazionale di Geofisica e Vulcanologia, Palermo, Italy
[5]Institut für Physik der Atmosphäre, Deutsches Zentrum für Luft- und Raumfahrt e.V. (DLR), Oberpfaffenhofen, Germany
[6]Meteorologisches Institut, Ludwig-Maximilians-Universität (LMU), München, Germany

Correspondence to: André Butz (andre.butz@dlr.de)

Received: 29 July 2016 – Published in Atmos. Meas. Tech. Discuss.: 8 September 2016
Revised: 2 December 2016 – Accepted: 14 December 2016 – Published: 2 January 2017

Abstract. Remote sensing of the gaseous composition of non-eruptive, passively degassing volcanic plumes can be a tool to gain insight into volcano interior processes. Here, we report on a field study in September 2015 that demonstrates the feasibility of remotely measuring the volcanic enhancements of carbon dioxide (CO_2), hydrogen fluoride (HF), hydrogen chloride (HCl), sulfur dioxide (SO_2), and bromine monoxide (BrO) in the downwind plume of Mt. Etna using portable and rugged spectroscopic instrumentation. To this end, we operated the Fourier transform spectrometer EM27/SUN for the shortwave-infrared (SWIR) spectral range together with a co-mounted UV spectrometer on a mobile platform in direct-sun view at 5 to 10 km distance from the summit craters. The 3 days reported here cover several plume traverses and a sunrise measurement. For all days, intra-plume HF, HCl, SO_2, and BrO vertical column densities (VCDs) were reliably measured exceeding 5×10^{16}, 2×10^{17}, 5×10^{17}, and 1×10^{14} molec cm^{-2}, with an estimated precision of 2.2×10^{15}, 1.3×10^{16}, 3.6×10^{16}, and 1.3×10^{13} molec cm^{-2}, respectively. Given that CO_2, unlike the other measured gases, has a large and well-mixed atmospheric background, derivation of volcanic CO_2 VCD enhancements (ΔCO_2) required compensating for changes in altitude of the observing platform and for background concentration variability. The first challenge was met by simultaneously measuring the overhead oxygen (O_2) columns and assuming covariation of O_2 and CO_2 with altitude. The atmospheric CO_2 background was found by identifying background soundings via the co-emitted volcanic gases. The inferred ΔCO_2 occasionally exceeded 2×10^{19} molec cm^{-2} with an estimated precision of 3.7×10^{18} molec cm^{-2} given typical atmospheric background VCDs of 7 to 8×10^{21} molec cm^{-2}. While the correlations of ΔCO_2 with the other measured volcanic gases confirm the detection of volcanic CO_2 enhancements, correlations were found of variable significance (R^2 ranging between 0.88 and 0.00). The intra-plume VCD ratios ΔCO_2 / SO_2, SO_2 / HF, SO_2 / HCl, and SO_2 / BrO were in the range 7.1 to 35.4, 5.02 to 21.2, 1.54 to 3.43, and 2.9×10^3 to 12.5×10^3, respectively, showing pronounced day-to-day and intra-day variability.

1 Introduction

The gaseous composition of non-eruptive, passively degassing volcanic plumes is largely dominated by water vapor (H_2O), carbon dioxide (CO_2), sulfur dioxide (SO_2), hydrogen sulfide (H_2S), and halogen bearing compounds such as hydrogen fluoride (HF), hydrogen chloride (HCl), and bromine monoxide (BrO). The relative abundances of the constituents vary with the type of volcano and magmatic

composition, the contributing degassing mechanisms, and the dynamics of mass transport in the volcano interior. Thus, monitoring volcanic gas emissions can help constrain subsurface processes and estimate fluxes of the geological carbon cycle (e.g., Allard et al., 1991; Goff et al., 2001; Burton et al., 2013). Furthermore, it holds the promise for improved eruption forecast since enhanced CO_2 / SO_2 emission ratios have been shown to precede eruptive volcanic activity with a lead time of hours to weeks (e.g., Aiuppa et al., 2007, 2010).

While remote sensing of volcanic plume composition has been demonstrated to be a valuable tool for various gases including HF, HCl, SO_2, and BrO (e.g., Mori et al., 1993; Love et al., 1998; Francis et al., 1998; Bobrowski et al., 2003; Grutter et al., 2008; Stremme et al., 2011, 2012; Theys et al., 2013), measuring volcanic CO_2 remotely faces the particular challenge to discriminate the volcanic enhancements from the background concentration of about 400 ppm (parts per million per volume). Therefore, measurement techniques for volcanic CO_2 mostly rely on in situ gas analyzers (e.g., Shinohara et al., 2008), open-path or closed-path spectroscopic techniques (e.g., Burton et al., 2000; Gerlach et al., 2002) deployed in the proximity of the source region, thereby avoiding downwind dilution of the plume. However, deployment close to the source typically comes with great costs and logistics effort, various hazards for instruments and operators, and, depending on the employed sampling strategy, limited representativeness for the volcanic source as a whole. Pioneering remote sensing experiments relied on detecting the absorption of volcanically emitted CO_2 along an atmospheric light path using the infrared emission of hot volcanic material (Naughton et al., 1969; Mori and Notsu, 1997) or exploiting the thermal contrast between the hot volcanic plume and the background sky (Goff et al., 2001). Aiuppa et al. (2015) demonstrated a LIDAR technique for scanning a volcanic CO_2 plume. However, these remote sensing techniques require path-integrated CO_2 enhancements in excess of several ppm or thermal contrast of several degrees between the plume and the background.

Here, we demonstrate that our field-deployable spectroscopic instrumentation enables remote sensing of volcanic CO_2 enhancements simultaneously with co-emitted HF, HCl, SO_2, and BrO. Our setup builds on direct-sunlight spectroscopy using portable spectrometers that sample the plume several kilometers downwind of Mt. Etna's craters. The key enabling element is the Fourier transform spectrometer (FTS) EM27/SUN that allows for measuring path-integrated CO_2 enhancements well below 1 ppm exploiting shortwave-infrared (SWIR) absorption bands (Gisi et al., 2012; Hase et al., 2015; Frey et al., 2015; Klappenbach et al., 2015). The FTS also allows for measuring path-integrated HF and HCl concentrations. We operated two of the FTS, one stationary and another one on a small truck together with a co-mounted grating spectrometer targeting SO_2 and BrO in the ultraviolet (UV) spectral range. The mobile FTS and the UV spectrometer were fed by the same beam of direct sunlight from a custom-built solar tracker (Klappenbach et al., 2015). During a 3-week field campaign in September 2015, the truck carried the mobile remote sensing observatory to various sampling locations in the vicinity of Mt. Etna while the stationary FTS observed background variability for most of the time.

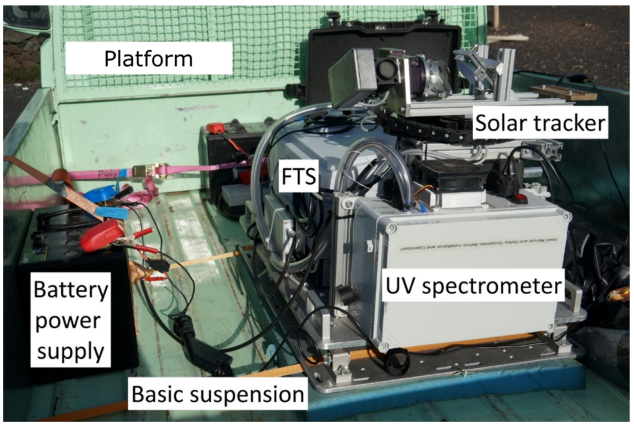

Figure 1. Photograph of the remote sensing observatory on the mobile platform, a small truck. The observatory consists of the Fourier transform spectrometer (FTS) EM27/SUN and the UV spectrometer ULS2048x64-ENV5. A common solar tracker feeds sunlight into the two spectrometers. The observatory sits on a rubber and foam suspension. A 12 V battery supplies power to the spectrometers, the solar tracker, two control laptops for the spectrometers, and a low-power consumption PC for the solar tracker.

2 Campaign deployment at Mt. Etna

Mt. Etna is a quiescently degassing volcano on Sicily, Italy, exhibiting four active summit craters in a confined source region above 3 100 m altitude. Typical passive, continuous non-eruptive degassing amounts to more than 5 kt of CO_2 per day (e.g., Aiuppa et al., 2008; Burton et al., 2013). Eruptive activity occurs occasionally but not during the campaign operations reported here, starting on 5 and ending on 25 September 2015. Whenever weather conditions were favorable for direct-sun view, the custom-built solar tracker, the mobile FTS, and the UV spectrometer were mounted on the truck. Figure 1 illustrates the setup of the mobile observatory. In the morning, the truck was taken to a location where visual inspection of the sky indicated Etna's plume roughly overhead. During sunrise, at large solar zenith angles, the observatory remained stationary collecting absorption spectra while the sun was rising. Later, at smaller solar zenith angles, we operated the observatory in stop-and-go patterns to collect scans through the volcanic plume. Operations were suspended whenever the sun was obscured by cloud cover, which persisted for several days in early September due to rainy conditions. Generally, cloud cover appeared around local noon. The early phase of the campaign was dedicated to testing the setup and identifying suitable measurement pro-

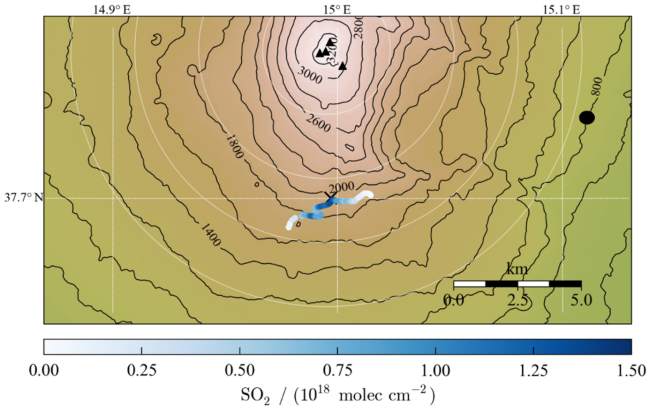

Figure 2. Topographic map of the southern slope of Mt. Etna. The background color shading corresponds to surface elevation with black contours in steps of 200 m altitude change. The white circular grid illustrates horizontal distances from the crater region in steps of 2.5 km as indicated by the ruler in the lower right. The four active craters on the summit at about 3300 m altitude are indicated by black triangles and the base station at Milo is illustrated by the black circle on the eastern slope. The blueish trajectory in the middle of the map shows the motion of the mobile observatory on 22 September, between 08:00 and 08:50 h UTC (typical solar zenith angle SZA = 55°) in the vicinity of Rifugio G. Sapienza (black cross). The color code is a rough measure for the observed SO_2 VCDs as indicated by the color bar. Note that SO_2 VCDs are plotted at the position of the observer at the time of measurement.

cedures. In total, we report on 3 days (18, 22, 23 September 2015) in the second half of the campaign, for which we focus on stop-and-go patterns in the vicinity of Rifugio G. Sapienza (37.700° N, 14.999° W; 1910 m a.s.l.) at the southern slope of Mt. Etna. The typical distance between the volcanic source region at the summit and the positions of the sun-viewing spectrometers amounted to 5–10 km. Figure 2 shows an illustrative trajectory of the truck on 22 September 2015. Since the truck was restricted to use general purpose roads, deployment options were limited and it was impossible to collect cross sections that were strictly perpendicular to the plume direction. Figure 2 also demonstrates that, due to rough topography in the vicinity of Mt. Etna, lateral displacements of the truck imply changes in observer altitude. Note that the mobile spectrometers were deployed south of the craters in such a way that the observation vectors towards the sun had southward components, sampling the plume at greater distances than the deployment locations. In addition to the mobile observatory, we operated another FTS at our base station in Milo (37.731° N, 15.113° W; 806 m a.s.l.) at the eastern slope of Mt. Etna. For the days reported here, the stationary FTS mostly observed background air masses providing a reference for the background variability of CO_2.

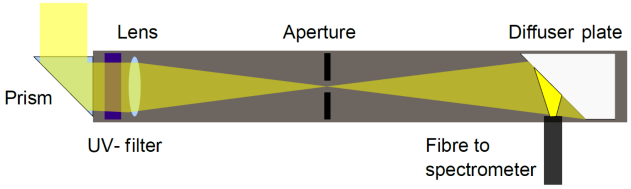

Figure 3. Sketch of the telescope used to feed sunlight into the UV spectrometer. The telescope was mounted into the outer part of solar light beam collected by the solar tracker. A prism feeds sunlight into the telescope (0.5 in. tube diameter, ∼ 120 mm tube length), which consists of a UV filter (Hoya U330), a lens (focal length $f = 40$ mm), and a circular aperture (800 µm diameter) aligned to the focus of the lens. A polytetrafluoroethylene (PTFE) diffuser plate illuminates the glass fiber (400 µm diameter), which then guides the sunlight into the UV spectrometer.

3 Instrumentation

Both the mobile and the stationary FTS are of the type EM27/SUN developed by Bruker Optics and the Karlsruhe Institute of Technology. The EM27/SUN delivers solar absorption spectra at a spectral resolution of 0.5 cm^{-1} in the range 5000 to 11 000 cm^{-1} without the need for detector cooling. Gisi et al. (2012), Hase et al. (2015), and Frey et al. (2015) showed that stationary deployment of the EM27/SUN enables measuring the CO_2 column concentrations with high accuracy and precision. Klappenbach et al. (2015) detailed the performance of the mobile instrument used here, for deployment on a research vessel. Previous studies typically co-added 10 double-sided interferograms with a total exposure of roughly 60 s. We adopted the same measurement pattern for the stationary FTS, but for the mobile FTS we processed pairs of double-sided interferograms with a total exposure of 12 s in order to keep temporal averaging small and to increase measurement frequency. The total field of view of the FTS amounts to 0.27°, resulting in the central part of the solar disk being observed.

The UV grating spectrometer is an AvaSpec-ULS2048x64-ENV5 manufactured by Avantes. It features a 1800 lines mm^{-1} grating and 2048 pixel linear array CCD detector covering the spectral range 294 to 457 nm. The entrance slit of the spectrometer is 200 µm wide, supporting an optical resolution of 0.8 nm (FWHM). The spectrometer is placed inside a housekeeping box (EnviMeS TSE 1.1) equipped with a Peltier cooling that keeps the spectrometer temperature stable at 15.00° C with a precision of 0.02° C. The housekeeping box disposes of a glass fiber coupling that allows for externally connecting a glass fiber for light intake without the need to open the box. During our campaign, the exposure times for individual spectra under clear sky were around 15 ms. Typically, we co-added 30 spectra, leading to effective exposures of several hundred milliseconds.

While the stationary FTS was equipped with the standard solar tracker delivered by Bruker Optics (Gisi et al.,

2011), the mobile observatory used a custom-built variant, initially developed for mobile applications by Klappenbach et al. (2015) and further enhanced here, to improve on the response times and to feed the mobile FTS and the UV spectrometer with the same light beam. Two rotatable tracking mirrors direct a light beam of 40 mm diameter into the mobile FTS through a wedged window. Given that the FTS only uses the central part of the beam, a portion of the outer part of the beam is fed into the UV spectrometer through a telescope. Figure 3 shows a sketch of the telescope assembly. A prism (10 mm side length) reflects the incoming sunlight into a 0.5 in. lens tube mounted on a kinematic platform (not shown). The light beam first passes a UV filter (Hoya U330) that shields unused parts of the solar spectrum, then a lens (focal length $f = 40$ mm) focuses the beam on an 800 µm wide circular aperture. Further downstream, a polytetrafluoroethylene (PTFE) diffuser plate illuminates a 400 µm glass fiber that takes the light into the spectrometer box via the fiber coupling. To support optical alignment, the length of the lens tube is adjustable, the prism can be rotated, and the attitude of the whole telescope can be controlled through the kinematic mount. Compared to previous stationary and ship-borne applications, volcanic CO_2 plume detection benefited from enhancing the response time of the solar tracker. At moderate driving speed (up to $\sim 30\,\mathrm{km\,h^{-1}}$) of the platform and benign road surface, the solar tracker was able to reliably stay on target (the sun) while driving and tracking stability was sufficient to enable recording of absorption spectra by the fast UV spectrometer. Real-time analysis of the SO_2 absorption signal on the passenger seat guided the stop-and-go patterns. However, tracking stability while driving was not sufficient to record CO_2 absorption spectra by the mobile FTS, which has substantially longer exposures than the UV spectrometer. Thus, all CO_2 measurements discussed here were recorded while the truck was stopped.

4 Data analysis

The solar absorption spectra recorded by the FTS and the UV spectrometer provide information on the gas concentrations, integrated along the path from the sun to the ground-based observer. We first retrieved the column gas abundances of CO_2, HF, and HCl from the SWIR (Sect. 4.1) and the abundances of SO_2 and BrO from the UV spectra (Sect. 4.2). Then, we inferred the volcanic enhancements (Sect. 4.3).

4.1 Spectral retrieval in the SWIR

The FTS delivered interferograms, from which we generated absorption spectra through Fourier transformation assuming Norton–Beer's medium strong apodization function (Norton and Beer, 1977). The DC part of the interferogram is a good measure for brightness fluctuations of the light source during recording of the interferogram. As described in Klappenbach et al. (2015), we used the DC part to discard spectra which suffered from variable illumination due, for example, to unstable tracking of the sun or thin clouds passing by. Small fluctuations of the DC part that passed our quality filter were corrected as described in Keppel-Aleks et al. (2007). In addition to the interferograms with severe brightness fluctuations, we discarded FTS measurements in cases of generally inferior quality of the spectra (as judged on basis of fitting residuals) and unsuccessful convergence of the spectral retrieval. Overall, the quality filtering removed virtually all the spectra recorded by the mobile FTS while the truck was moving.

Table 1. Spectral retrieval windows and their properties used for processing the FTS absorption spectra in the SWIR. Parentheses following absorber molecules indicate the used spectroscopic databases: TCCON refers to the spectroscopic database used by the Total Carbon Column Observing Network (Toon, 2014), HITRAN2008 refers to Rothman et al. (2009), and HITRAN2009 refers to Rothman et al. (2009) with published updates and our own empirical modifications. LM refers to the line-mixing database by Lamouroux et al. (2010) used as a correction to HITRAN2008.

Spectral range ($\mathrm{cm^{-1}}$)	Target absorbers	Interfering absorbers
7765–8005	O_2 (TCCON), HF (HITRAN2008)	H_2O (HITRAN2009), O_2–O_2 (TCCON)
6308–6390	CO_2 (LM)	H_2O (HITRAN2009) CH_4 (HITRAN2008)
6173–6276	CO_2 (LM)	H_2O (HITRAN2009) CH_4 (HITRAN2008)
5684–5795	HCl (HITRAN2008)	CH_4 (HITRAN2008) H_2O (HITRAN2009)

After generation of the absorption spectra, a line-by-line atmospheric transmittance model retrieved the concentrations of the target gases integrated along the vertical, the vertical column densities (VCDs). We employed the software package PROFFIT developed for ground-based direct-sun spectroscopy (Hase et al., 2004) and previously used for processing EM27/SUN spectra (Gisi et al., 2012; Frey et al., 2015; Hase et al., 2015; Klappenbach et al., 2015). PROFFIT evaluates Beer–Lambert's law assuming a curved hydrostatic atmosphere with horizontally homogeneous layers. We considered several spectral windows in the SWIR with various absorbing molecules as detailed in Table 1. Molecular absorption was taken into account through a Voigt line-shape model including corrections due to line mixing for CO_2. Table 1 also lists the databases for the driving spectroscopic parameters. An empirical line list modeled the solar Fraunhofer lines. The parameters to be estimated for each measurement comprised scaling factors for the vertical a priori profiles of the absorbers and auxiliary parameters such as spectral shift parameters per window and parameters to fit the transmittance baseline. For CO_2, HCl, and HF, we only scaled the lower tropospheric part of the vertical profile (four layers be-

tween 3.2 and 4.9 km altitude) and adopted the a priori for the rest. VCDs are a posteriori calculated by summing up the layers of the scaled vertical profiles. The volcanic VCD enhancements discussed below thus assume the case of a horizontally homogeneous, extended plume.

Since the molecular absorption lines in the SWIR are optically thick as well as pressure and temperature dependent, the spectral retrieval in the SWIR (unlike DOAS (differential optical absorption spectroscopy) in the UV) requires a detailed representation of the vertical profiles of meteorological parameters and gas concentrations. The profiles of pressure, temperature, and humidity were derived from global NCEP (National Centers for Environmental Prediction) fields on $1\,^\circ \times 1^\circ$ (latitude $\times$ longitude) via interpolation in space and time. Surface pressure, surface elevation, latitude and longitude of the soundings were measured by pressure transducers and GPS recorders deployed next to the FTS and subsequently used to construct the input meteorological profiles and the a priori absorber profiles. For O_2 and H_2O, the latter were taken from the meteorological pressure and humidity data. For CO_2, HCl, HF, and CH_4, we used climatological profiles taken from the recommendations of the Infrared Working Group (IRWG) of the Network for the Detection of Atmospheric Composition Change (NDACC) for the mid-latitudes. Note that all retrievals irrespective of sampling intra-plume or background conditions assumed background absorber profiles; i.e., the retrieval had no a priori information on the volcanic plume except for the fact that we only allowed for scaling of the lower tropospheric part of the vertical profile.

4.2 Spectral retrieval in the UV

The spectral retrieval for the soundings of the UV spectrometer was based on the DOAS technique (Platt and Stutz, 2008). It builds on Beer–Lambert's law and exploits narrow-band absorption bands of optically thin absorbers like SO_2 and BrO. Table 2 lists details of the spectral windows and the absorption cross sections used for the target gas retrieval. The tabulated high-spectral-resolution absorption cross sections were convolved by the instrument spectral response function and then used to fit the recorded transmittance spectra after subtraction of dark current and offset spectra. A least-squares fitting routine determined the target absorber concentrations integrated along the slant light path through the atmosphere, the slant column densities (SCDs). Ancillary fitting parameters were a cubic background polynomial, a linear additive offset accounting for spectrometer stray light as well as the SCDs of interfering absorbers ozone (O_3), nitrogen dioxide (NO_2), the oxygen collisional complex (O_2–O_2), and formaldehyde (CH_2O). UV spectra were discarded in cases of unstable temperature of the spectrometer and strong intensity fluctuations between adjacent spectra.

To compare the UV-retrieved SCDs with the VCDs retrieved in the SWIR, we translated the SO_2 and BrO SCDs into VCDs. To this end, we approximated the geometric assumptions of the SWIR retrieval by ratioing the SCDs by the air mass factor $\frac{1}{\cos(\mathrm{SZA})}$ (solar zenith angle, SZA). If the volcanic plume was horizontally extended and if our lines of sight crossed the plume perpendicularly to its propagation direction, the reported VCDs were truly representative of the vertical column enhancement in the plume. If the volcanic plume has a more complicated geometric shape, that shape would need to be considered for inferring volcanic enhancements and volcanic emissions in absolute units. Ratios of the various gases as discussed below, however, are not affected by the geometric conversion since all gases were measured in the same light path.

4.3 Deriving volcanic VCD enhancements

Whenever we detected significant VCDs of SO_2, HCl, HF, and BrO, we considered those to be volcanic enhancements since atmospheric background concentrations of these species are small. Atmospheric CO_2, however, is a generally well-mixed gas with background concentrations of roughly 400 ppm ($\mathrm{VCD} \sim 8.5 \times 10^{21}$ molec cm^{-2} at 1 bar surface pressure). Therefore, determining volcanic CO_2 enhancements faces the challenges that (A) the measured VCDs co-vary with surface pressure, for our setup mainly variable due to variable observer altitude, and (B) the atmospheric background needs to be removed. We addressed challenge (A) by simultaneously retrieving the VCD of molecular oxygen (O_2) and calculating the column-averaged dry-air mixing ratio XCO_2 via

$$\mathrm{XCO_2} = \frac{[\mathrm{CO_2}]}{[\mathrm{O_2}]} \times 0.20942, \quad (1)$$

where square brackets indicate observed VCDs and 0.20942 is the atmospheric O_2 mole fraction. Referencing by retrieved O_2 is a standard method that aims at canceling instrumental effects and retrieval artefacts (e.g., Wunch et al., 2010; Klappenbach et al., 2015). Assuming that a change in observer altitudes causes the same relative change in the O_2 and CO_2 VCDs, XCO_2 derived from Eq. (1) is independent of observer altitude and, thus, serves to address challenge (B).

The atmospheric XCO_2 background varies due to variable meteorological conditions transporting distant source–sink signals to Mt. Etna. Further, imperfect knowledge of spectroscopic parameters and other instrumental or retrieval effects can cause a spurious dependence of XCO_2 on viewing geometry (e.g., Klappenbach et al., 2015). Therefore, we fitted a function P linear in time to the background XCO_2 records. Background soundings are the ones collected at most 30 min before or after a plume scan and with small HF VCDs ($[\mathrm{HF}] < 1 \times 10^{16}$ molec cm^{-2}). Intra-plume measurements are those in-between background soundings exceeding the HF threshold. The volcanic column-averaged mixing

Table 2. Spectral retrieval windows and their properties used for processing the absorption spectra in the UV. Brackets following absorber molecules indicate the reference temperatures at which the absorption cross sections were measured in the laboratory. Parentheses contain references to the relevant data sources.

Spectral range (nm)	Target absorbers	Interfering absorbers
312.0–326.8	SO_2 [298 K] (Vandaele et al., 2009)	O_3 [221 K] (Burrows et al., 1999)
330.6–352.8	BrO [298 K] (Fleischmann et al., 2004)	SO_2 [298 K] (Vandaele et al., 2009)
		O_3 [221 K] (Burrows et al., 1999)
		O_2–O_2 (Hermans et al., 2003)
		NO_2 [294 K] (Vandaele et al., 1998)
		CH_2O [298 K] (Meller and Moortgat, 2000)

ratio enhancement ΔXCO_2 then reads

$$\Delta\mathrm{XCO_2} = \mathrm{XCO_2} - P. \quad (2)$$

The volcanic VCD enhancement ΔCO_2 is given by

$$[\Delta\mathrm{CO_2}] = \Delta\mathrm{XCO_2} \times \frac{[\mathrm{O_2}]}{0.20942}. \quad (3)$$

Figures 4 through 6 illustrate the step-by-step derivation of volcanic ΔXCO_2 for the 3 considered days. The variation of the retrieved CO_2 VCDs (upper panels in Figs. 4 through 6) is mostly due to changes in observer altitude. On 18 September, the stop-and-go operations started at around 06:00 h UTC at high altitude close to Rifugio G. Sapienza corresponding to low CO_2 VCDs. The local roads then led the truck downhill toward the southwest causing increasing CO_2 VCDs until we returned to Rifugio G. Sapienza at the end of the morning at about 09:00 h UTC. On 22 September, stop-and-go patterns were restricted to the closer vicinity of Rifugio G. Sapienza (see also Fig. 2) with less altitude-induced changes in CO_2 VCDs than on the other days. On 23 September, observations started around 06:00 h UTC in stationary configuration at Rifugio G. Sapienza waiting for the sun to rise. Around 06:45 h UTC, we took up the stop-and-go patterns, which again led us down and back up Mt. Etna's southern slope until 09:00 h UTC.

Calculating XCO_2 according to Eq. (1) removes the altitude-induced variability in the observed CO_2 VCDs (middle panels in Figs. 4 through 6) and reveals distinct volcanic enhancements between the background measurements and for the sunrise observations on 23 September. Data scatter grows toward late morning, which might be due to some spectra with non-perfect solar tracking escaping our quality filters. Typically, clouds developed in late morning and disrupted the solar tracking. The XCO_2 records observed by the stationary FTS deployed at Milo on the eastern slope of Mt. Etna (blue crosses) confirm that the linear background polynomial (red) is well suited to account for background XCO_2 variability. Except for late morning on 23 September, the stationary FTS at Milo sampled background air masses (according to the HF threshold). On 23 September after about

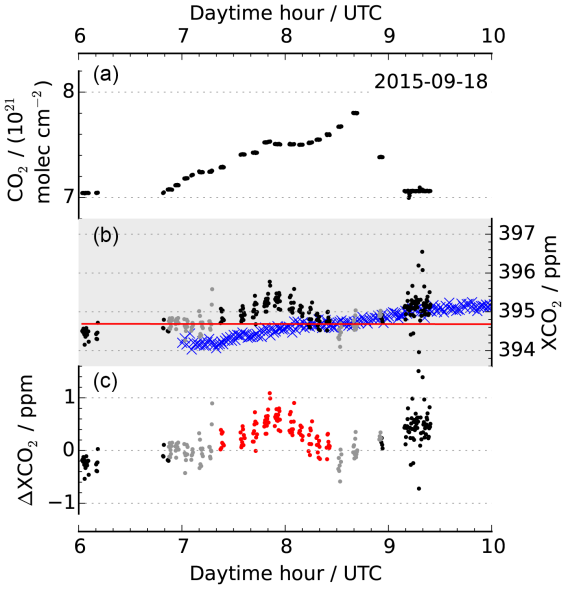

Figure 4. Derivation of ΔXCO_2 for the spectra collected by the mobile FTS on 18 September 2015. The upper panel shows the CO_2 VCDs retrieved by the spectral retrieval described in Sect. 4.1. The middle panel shows the column-averaged dry-air mixing ratio XCO_2 (black and grey dots) calculated via Eq. (1). Background measurements (grey) are used to fit the linear background polynomial illustrated by the red line. Blue crosses show the measurements collected by the stationary FTS at the eastern slope of Mt. Etna. The lower panel depicts the volcanic XCO_2 enhancement (ΔXCO_2) calculated according to Eq. (2). Red circles are considered intra-plume enhancements.

08:40 UT, the volcanic plume started drifting toward the lines of sight of the stationary FTS. We refrained from directly using the stationary measurements for background removal since the stationary FTS was placed at about 10 km distance from the truck trajectory at the eastern slope of the mountain. An improved setup might benefit from operating the stationary FTS closer to the trajectory of the mobile observatory.

Removing the background via Eq. (2) yields the volcanic enhancement ΔXCO_2 (lower panels in Figs. 4 through 6),

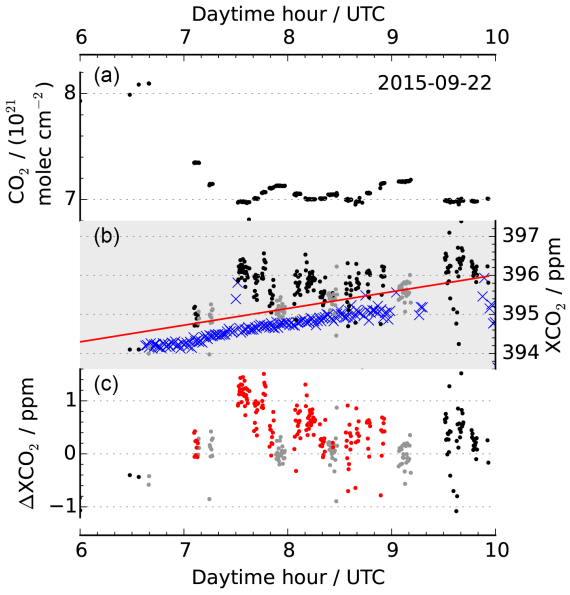

Figure 5. Same as Fig. 4 but for 22 September 2015.

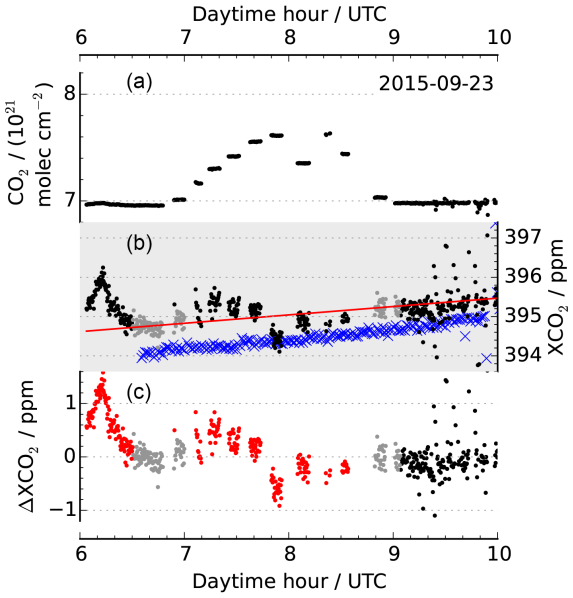

Figure 6. Same as Fig. 4 but for 23 September 2015.

which is further processed to yield the volcanic VCD enhancement according to Eq. (3).

5 Volcanic ΔCO_2, HF, HCl, SO_2, and BrO

Figures 7 through 9 collect time series of the volcanic enhancements of CO_2, HF, HCl, SO_2, and BrO found in the plume of Mt. Etna. Our mobile observatory detected the volcanic plume for a single stop-and-go traverse on 18 September, three traverses on 22 September, and another traverse as well as the sunrise measurements on 23 September. Since the truck carrying the observatory was constrained to use the local roads, the traverses were not strictly perpendicular to the plume but exhibited displacements along plume direction and in altitude (see also Fig. 2). Early on 18 September, for example, Etna's plume was sampled while the observatory was moving to the southwest until 08:00 h UTC, when a dead end forced us to turn back and to move the truck to the east.

We find volcanic ΔCO_2 occasionally exceeding 2×10^{19} molec cm^{-2}, which, depending on observer altitude, amounts to column-averaged mixing ratio enhancements of a few tenths of a ppm (see also lower panels in Figs. 4 through 6). Thus, given background VCDs of 7 to 8×10^{21} molec cm^{-2}, the detected volcanic signal corresponds to a sensitivity of about 1 : 400. We estimated the overall ΔCO_2 precision as a measure for the random error component by calculating the standard deviation (1σ) of all the background measurements identified via the HF threshold. It amounts to 3.7×10^{18} molec cm^{-2} for ΔCO_2 (0.20 ppm for ΔXCO_2), suggesting that individual measurements exceed the precision estimate by a factor 5 to 6. Detection of ΔCO_2 is corroborated by correlated enhancements in HF, HCl, SO_2, and BrO. Precision estimates for the latter species amount to 2.2×10^{15}, 1.3×10^{16}, 3.6×10^{16}, and 1.3×10^{13} molec cm^{-2}, respectively, where we first averaged the UV-measured SO_2 and BrO VCDs on the 12 s integration time of coincident FTS spectra and then calculated the standard deviation of the background measurements identified through the HF criterion.

Figure 10 further examines the correlation between ΔCO_2 and co-emitted SO_2 for the intra-plume measurements, while Figs. 11 through 13 show the correlations between SO_2 and HF, HCl, and BrO. As above the UV-measured SO_2 and BrO VCDs were averaged for the integration time of coincident FTS spectra. Table 3 summarizes the ΔCO_2 / SO_2, SO_2 / HF, SO_2 / HCl, and SO_2 / BrO VCD ratios (as well as R^2) obtained by fitting straight lines to the correlations. For 22 and 23 September, we investigated the correlations for all the intra-plume measurements of the respective day as well as for three subsets on each day. On 22 September, these subsets correspond to the three stop-and-go transects (before 08:00 h UTC, between 08:00 and 08:30 h UTC, after 08:30 h UTC). On 23 September, the correlations group into three subsets that can be attributed to the sunrise observations, the early stop-and-go operations (between 07:00 and 07:45 h UTC), and the later stop-and-go operations (after 07:45 h UTC).

The ΔCO_2 / SO_2 ratios show considerable day-to-day and intra-day variability ranging between 7.1 ± 1.5 and 35.4 ± 1.3 when considering the intra-day subsets. The errors correspond to the standard deviations of the fitted slopes. On 18 September, R^2 documents a good correlation between ΔCO_2 and SO_2. On 22 September, R^2 is fair for the two earlier plume transects but vanishes for the third transect and

Table 3. Intra-plume VCD ratios found by fitting a straight line to the correlations shown in Figs. 10 through 13. The errors are the standard deviations of the fitted slopes. The R^2 of the linear fit is shown in parentheses. On 22 and 23 September, we inferred VCD ratios for the whole day and three subsets separately. The lowermost row provides the campaign-averaged VCD ratios and standard deviations calculated from the daily subsets. The ΔCO_2 / SO_2 ratios for the measurements after 07:45 UTC (bracketed) on 23 September need to be considered with care since ΔCO_2 is negative. For details see text.

Date and time	ΔCO_2 / SO_2	SO_2 / HF	SO_2 / HCl	SO_2 / BrO $\times 10^3$
2015-09-18	14.3 ± 1.6 (0.45)	10.5 ± 0.3 (0.93)	2.38 ± 0.07 (0.94)	5.54 ± 0.12 (0.96)
2015-09-22	6.1 ± 2.4 (0.04)	5.60 ± 0.14 (0.91)	1.74 ± 0.04 (0.93)	3.35 ± 0.11 (0.86)
Before 08:00 h UTC	13.5 ± 3.3 (0.20)	6.53 ± 0.22 (0.93)	1.99 ± 0.04 (0.97)	4.68 ± 0.12 (0.96)
Between 08:00 and 08:30 h UTC	7.1 ± 1.5 (0.33)	6.50 ± 0.16 (0.97)	2.01 ± 0.05 (0.97)	3.75 ± 0.09 (0.97)
After 08:30 h UTC	0.40 ± 8.7 (0.00)	4.76 ± 0.13 (0.97)	1.54 ± 0.05 (0.96)	3.26 ± 0.18 (0.90)
2015-09-23	35.2 ± 2.3 (0.48)	7.33 ± 0.66 (0.32)	2.52 ± 0.09 (0.75)	2.93 ± 0.30 (0.28)
Sunrise	35.4 ± 1.3 (0.88)	21.2 ± 0.3 (0.98)	3.43 ± 0.03 (0.99)	12.5 ± 0.4 (0.92)
Between 07:00 and 07:45 h UTC	11.6 ± 2.8 (0.17)	10.9 ± 0.4 (0.89)	2.42 ± 0.05 (0.96)	4.84 ± 0.16 (0.92)
After 07:45 h UTC	[39.2 ± 6.9 (0.34)]	5.02 ± 0.37 (0.74)	1.54 ± 0.08 (0.86)	2.92 ± 0.19 (0.78)
Averages and standard deviation among the daily subsets	17 ± 14	9.3 ± 5.8	2.16 ± 0.65	5.4 ± 3.3

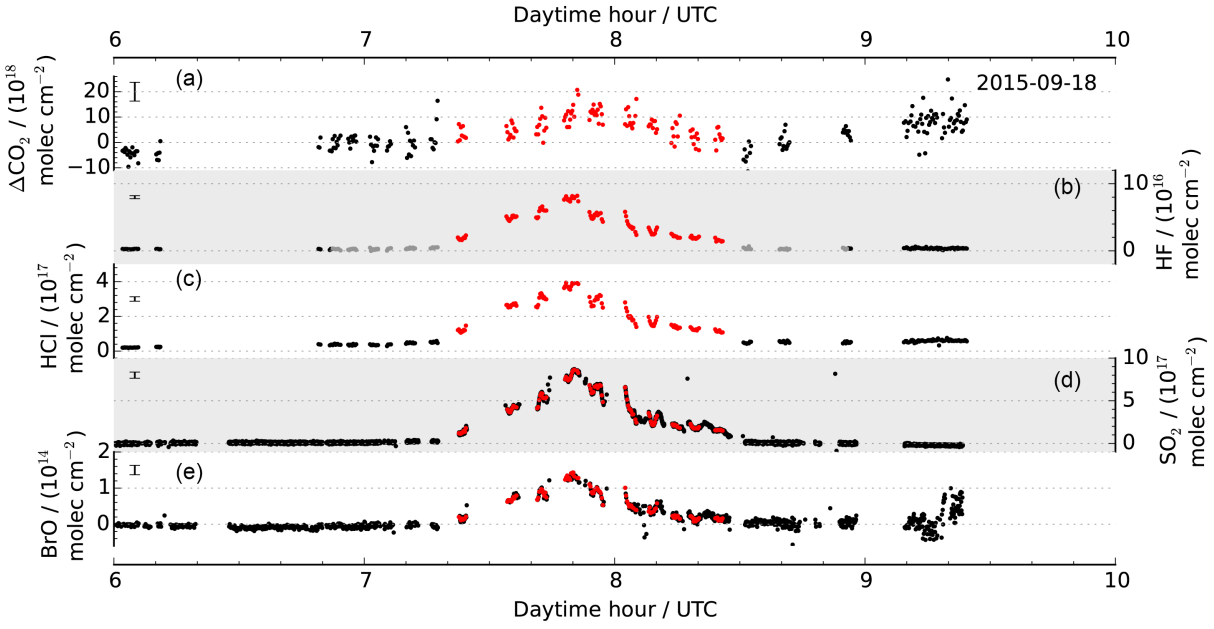

Figure 7. Time series of volcanic VCD enhancements in the plume of Mt. Etna observed on 18 September. ΔCO_2 (first panel, left ordinate) correlates with enhancements in HF (second panel, right ordinate), HCl (third panel, left ordinate), SO_2 (fourth panel, right ordinate), and BrO (fifth subpanel, left ordinate). Grey symbols for HF indicate background measurements. Red closed symbols indicate intra-plume soundings used for further interpretation. For the UV-measured species SO_2 and BrO, we only consider those intra-plume soundings that occur within the integration time of a coincident FTS measurement. Therefore, some SO_2 and BrO measurements that are clearly intra-plume are not red colored. The precision estimated from the standard deviation of all background soundings is shown as an error bar in the upper left corner of each panel.

for the case of a single correlation assumed valid for the whole day. The time series in Fig. 8 confirms that low outliers contaminate the ΔCO_2 record after 08:30 h UTC on 22 September, which might be due to emerging cloud cover disturbing solar tracking stability. On 23 September, we find good correlation for the sunrise observations and a fair R^2 for the early phase of the plume transect (between 07:00 and 07:45 h UTC). For the later phase of the transect (after 07:45 h UTC) ΔCO_2 is negative, which is unreasonable and possibly points to deficiencies of the CO_2 background

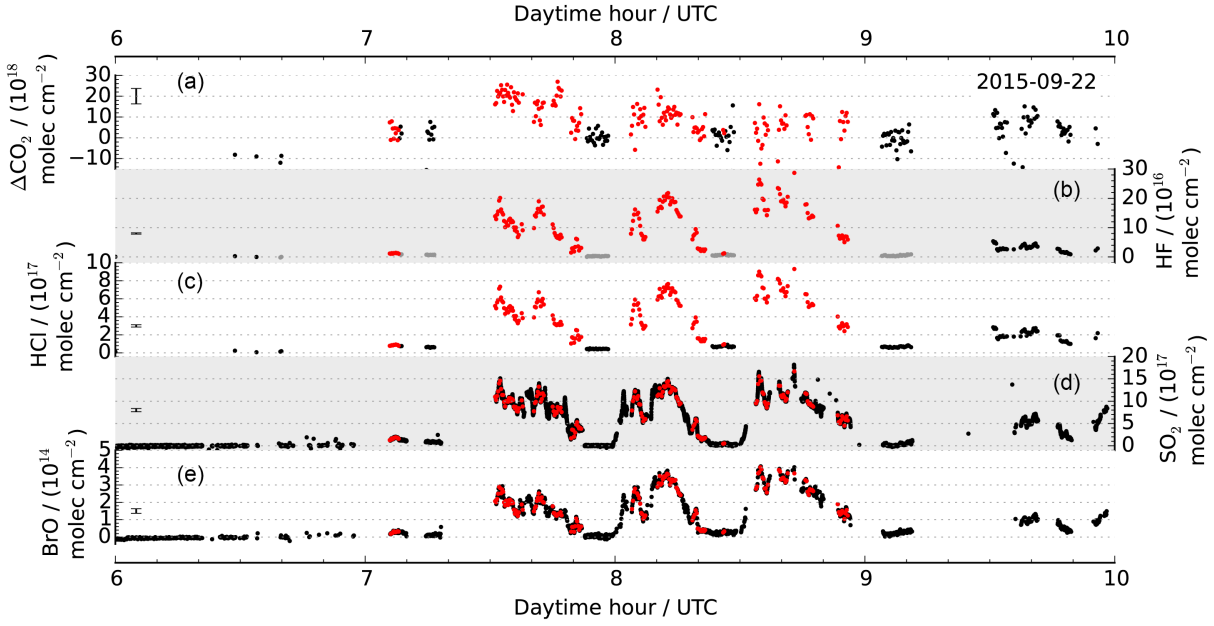

Figure 8. Same as Fig. 7 but for 22 September 2016.

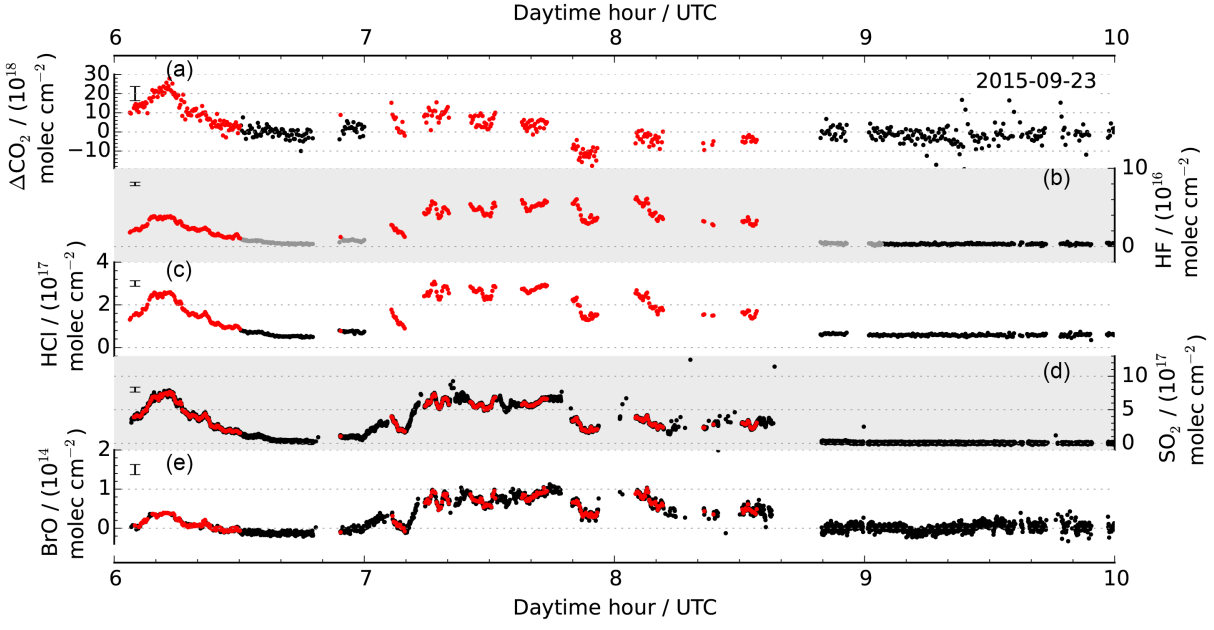

Figure 9. Same as Fig. 7 but for 23 September 2016.

removal as further discussed below. Assuming a single correlation for 23 September would clearly mask the geophysical variability contained in the records.

The SO_2 / HF, SO_2 / HCl, and SO_2 / BrO VCD ratios reveal high R^2 for all intra-day subsets. On 23 September there is considerable variability in the VCD ratios, which is supported by Figs. 11 through 13. The decreasing SO_2 / HF, SO_2 / HCl, and SO_2 / BrO ratios indicate that the composition of the sampled parts of the plume changed from relatively SO_2-rich to SO_2-poor in the course of the morning hours. The ΔCO_2 / SO_2 ratios also yield a substantial decrease between sunrise and the early stop-and-go operations (between 07:00 and 07:45 h UTC) but an increase later (after 07:45 h UTC). After 07:45 h UTC, however, ΔCO_2 is negative, which is unreasonable. Thus, we argue that, on 23 September, composition of the observed parts of the plume

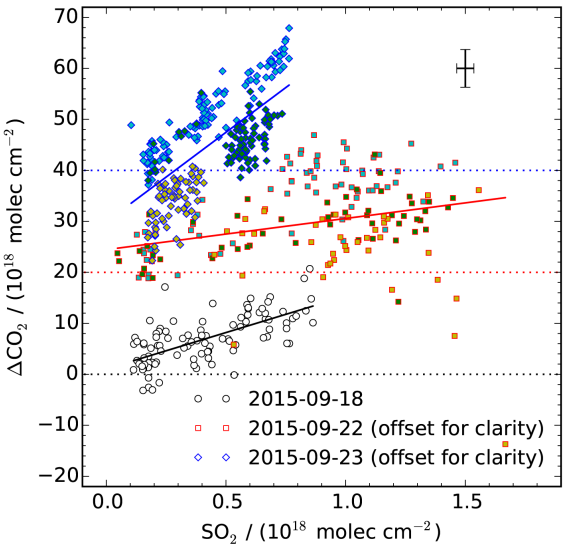

Figure 10. Correlation of ΔCO_2 and SO_2 intra-plume VCDs observed on 18 September (black circles), 22 September (red squares), and 23 September (blue diamonds) 2015. On 22 and 23 September, we identify three separate groups. On 22 September, these groups are data recorded before 08:00 h UTC (cyan filling), between 08:00 and 08:30 h UTC (green filling), and after 08:30 h UTC (yellow filling). On 23 September, these groups are data recorded during sunrise (cyan filling), after sunrise before 07:45 h UTC (green filling), and after 07:45 h UTC (yellow filling). The solid lines are fits to the daily records, fits for the intra-day subsets are omitted for clarity. The error bars in the upper right corner illustrate the precision estimated from the standard deviation of background soundings. For clarity, data on 22 and 23 September are offset in ordinate by 20×10^{18} and 40×10^{18} molec cm^{-2}, respectively, as indicated by the colored dotted lines.

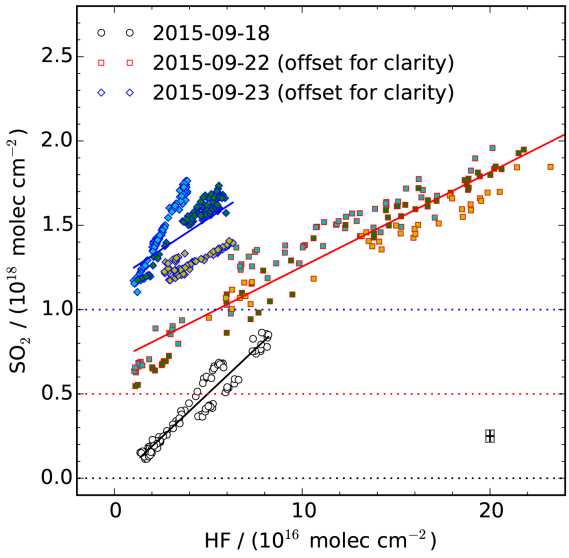

Figure 11. Same as Fig. 10 but for SO_2 and HF VCDs. For clarity, data on 22 and 23 September are offset in ordinate by 0.5×10^{18} and 1.0×10^{18} molec cm^{-2}, respectively, as indicated by the colored dotted lines.

changed from relatively SO_2-rich to SO_2-poor and, likewise, from relatively CO_2-rich to CO_2-poor while HF, HCl, and BrO levels remained relatively elevated. The argument is supported by the observations of the stationary FTS, which started detecting elevated HF levels at the eastern slope from 08:40 h UTC onward. This finding suggests that, in the later phase of the stop-and-go operations on the southern slope, the plume migrated away from the lines of sight of the mobile observatory toward the lines of sight of the stationary FTS deployed on the eastern slope. Most likely, this change went along with variable contributions of the various craters to the plume composite observed by the mobile FTS.

Given the detected composition variability for 23 September, the negative ΔCO_2 found after 07:45 h UTC could be an artefact of the CO_2 background removal, which is based on the HF threshold for identifying background soundings. If our spectrometers sampled a CO_2-rich (and HF-rich) plume in the early morning and a CO_2-poor (but HF-rich) plume later, HF would be a poor CO_2-plume indicator for the later period and the negative ΔCO_2 could just correspond to undetectably low enhancements. To try the sensitivity of the inferred ΔCO_2 to background removal on 23 September, we deliberately categorized all CO_2 measurements after 07:45 h UTC as background and recalculated ΔCO_2 as described in Sect. 4.3. The inferred ΔCO_2 / SO_2 ratios for sunrise and for the early stop-and-go operations (between 07:00 and 07:45 h UTC) remain largely unchanged, amounting to 34.8 ± 0.9 ($R^2 = 0.88$) and 12.7 ± 2.7 ($R^2 = 0.21$), respectively. Thus, our conclusions for the early measurements on 23 September are largely insensitive to background removal. Overall, our assessment emphasizes that short-term composition variability of the observed plume requires careful consideration.

6 Discussion and conclusion

We demonstrate simultaneous remote sensing of volcanic CO_2 (ΔCO_2), HF, HCl, SO_2, and BrO VCD enhancements in the plume of quiescently degassing Mt. Etna several kilometers downwind of the source. Our remote sensing observatory combined the portable and rugged EM27/SUN FTS for the SWIR spectral range (observing CO_2, HF, HCl) with a DOAS spectrometer for the UV (observing SO_2, BrO), both instruments measuring direct-sun absorption spectra. The spectrometers were supplied with sunlight by a common, fast solar tracker, all together deployed on a mobile platform and supplied by a 12 V battery. The mobile setup enabled sequentially measuring intra-plume and background air masses in stop-and-go patterns. Campaign operations were supported by another, stationary, EM27/SUN FTS, sampling atmospheric background conditions for most of the time. Gener-

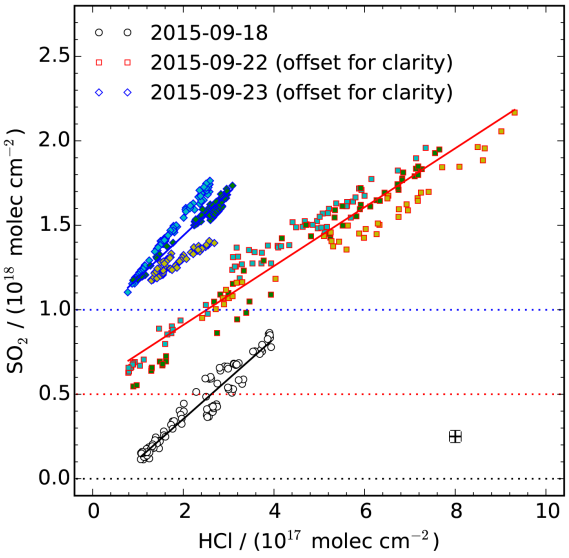

Figure 12. Same as Fig. 10 but for SO_2 and HCl VCDs. For clarity, data on 22 and 23 September are offset in ordinate by 0.5×10^{18} and 1.0×10^{18} molec cm^{-2}, respectively, as indicated by the colored dotted lines.

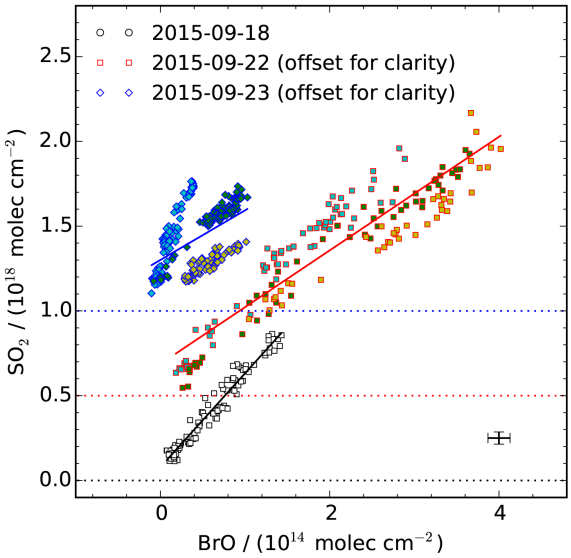

Figure 13. Same as Fig. 10 but for SO_2 and BrO VCDs. For clarity, data on 22 and 23 September are offset in ordinate by 0.5×10^{18} and 1.0×10^{18} molec cm^{-2}, respectively, as indicated by the colored dotted lines.

ally, we focused on the retrieval of ΔCO_2, since CO_2, unlike the other measured volcanic gases, has a high atmospheric background concentration that is well mixed.

For 3 days reported here, the sunrise and stop-and-go observations yielded ΔCO_2 up to about 2×10^{19} molec cm^{-2} with an estimated precision of 3.7×10^{18} molec cm^{-2}. The other volcanic gases were measured with an estimated precision of 2.2×10^{15}, 1.3×10^{16}, 3.6×10^{16}, and 1.3×10^{13} molec cm^{-2}, for HF, HCl, SO_2, and BrO, respectively. The key to detecting the small volcanic ΔCO_2 enhancements on top of the high atmospheric CO_2 background column (7 to 8×10^{21} molec cm^{-2}) was the simultaneous observation of the overhead O_2 column and of volcanic HF coemitted with CO_2. The O_2 column was used to compensate CO_2 variations due to changes in observer altitude. The HF columns provided an indication for intra-plume and background measurements. The latter were used to remove the atmospheric CO_2 background. The tightest correlation between ΔCO_2 and SO_2 ($R^2 = 0.88$) was found for the sunrise observations on 23 September, when the slant absorption path through the atmosphere was longest among our campaign records. Good to fair correlations (R^2 in the range 0.45 to 0.17) were found for four stop-and-go plume transects. One plume transect yielded a vanishing correlation between ΔCO_2 and SO_2 and another plume transect yielded negative ΔCO_2, most likely related to a change of plume composition from CO_2-rich to CO_2-poor during the transect. The correlations between SO_2 and HF, SO_2 and HCl, and SO_2 and BrO were all high (R^2 greater than 0.9 for all except one transect).

The intra-plume VCD ratios of ΔCO_2 / SO_2, SO_2 / HF, SO_2 / HCl, and SO_2 / BrO match the range of emission ratios and molar ratios previously reported for Mt. Etna (e.g., Aiuppa et al., 2007, 2008; La Spina et al., 2010; Voigt et al., 2014). During our campaign operations, in situ gas analyzers deployed in the vicinity of the summit craters found molar CO_2 / SO_2 ratios of 17.7 ± 10.3 close to Voragine crater on 18 September, 22.2 ± 5.8 close to Bocca Nuova crater on 22 September, and 13 ± 5 close to Bocca Nuova crater on 23 September, which confirms that Mt. Etna exhibits substantial variability of the emissions and that the various craters show different emission ratios (e.g., Aiuppa et al., 2008; La Spina et al., 2010). Since our remote sensing approach samples the plume several kilometers downwind of the craters, variability of the observed plume composition can be either due to temporally variable source gas emission, varying contributions of the different craters (e.g., induced by variable winds) (Voigt et al., 2014), and possibly flank emissions contributions (Allard et al., 1991) to the plume. Interpretation of our remote sensing data records becomes difficult if such variability occurs on the timescales of a plume transect. For our measurements on 23 September, we find a change in plume composition from CO_2-rich and SO_2-rich to CO_2-poor and SO_2-poor in the course of the morning hours. Most likely, the detected trend occurred since plume direction changed from southward to eastward, which caused variable contributions of the various craters to the plume composite observed on the southern slope of Mt. Etna.

The employed methodology bares potential for substantial extension and refinement. In view of plume variability, data interpretation would benefit from reducing the time span needed to conduct plume transects by the mobile observatory. During our campaign, the fastest transects took roughly

30 min. Reducing the exposure time of the FTS or the number of spectra collected during a transect would speed up the operations but the signal-to-noise ratio would become worse. A caveat also applies to variability of the volcanic CO_2, HF, or HCl signal on the timescale of the FTS exposure (12 s for the mobile FTS, 60 s for the stationary FTS). Since the FTS collects interferograms, a change of the volcanic gas signal during interferogram recording has a largely unpredictable effect on the absorption spectra and the inferred gas columns. A grating spectrometer would in good approximation average the volcanic signal over the exposure time. In the view of extending our methodology toward emission estimates, we will aim at linking the VCD ratios observed in the plume to actual emission ratios by combining our measurements with the monitoring infrastructures at Mt. Etna such as the FLAME SO_2 network (Salerno et al., 2009), by operating a dedicated SO_2 camera system together with the direct-sun spectrometers (e.g., Kern et al., 2015; D'Aleo et al., 2016), or by meteorological modeling of the local wind fields. In the view of volcano monitoring, a few of our spectrometers could be operated in stationary observatories, possibly together with a mobile observatory, to set up a network that allows for monitoring Mt. Etna's or any other suitable volcano's plume. If the FTS can be deployed somewhat closer to the source than the local infrastructures allowed for during our campaign, the plume would be less diluted and ΔCO_2 would show greater enhancements, allowing for better relative precision than reported here.

Overall, our approach allows for detecting volcanic CO_2 enhancements with good confidence and for measuring volcanic HF, HCl, SO_2, and BrO with high precision using a setup that can be easily deployed in the field in safe distance from the craters. Therefore, further refinements such as discussed above could make our approach a valuable tool in volcano monitoring. Inevitable drawbacks of direct-sun spectroscopy, however, are the required daytime and clear-sky conditions.

7 Data availability

The data are available from the author upon request.

Author contributions. Nicole Bobrowski and André Butz developed the research question. André Butz, Anna Solvejg Dinger, Nicole Bobrowski, Julian Kostinek, Lukas Fieber, Constanze Fischerkeller, Giovanni Bruno Giuffrida, Jonas Kuhn, Peter Lübcke, and Lukas Tirpitz took an active part in the field campaign by operating instrumentation, collecting, analyzing, and sharing data. Frank Hase and Friedrich Klappenbach supported preparations for the field campaign through instrument developments. André Butz, Anna Solvejg Dinger, Nicole Bobrowski, Frank Hase, Friedrich Klappenbach, and Qiansi Tu contributed to the spectral retrievals. André Butz wrote the paper. Anna Solvejg Dinger produced the figures for an earlier version of the manuscript.

Acknowledgements. We acknowledge support by the Heidelberg Karlsruhe Research Partnership (HEiKA) under project "Accurate Prototype remote sensing of correlated carbon and sulfur emissions from mount Etna (APE)" and Deutsche Forschungsgemeinschaft (DFG) under the Emmy-Noether project "RemoteC" (BU2599/1-1). The data are available upon request from the authors.

The article processing charges for this open-access publication were covered by a Research Centre of the Helmholtz Association.

Edited by: D. Griffith
Reviewed by: one anonymous referee

References

Aiuppa, A., Moretti, R., Federico, C., Giudice, G., Gurrieri, S., Liuzzo, M., Papale, P., Shinohara, H., and Valenza, M.: Forecasting Etna eruptions by real-time observation of volcanic gas composition, Geology, 35, 1115–1118, doi:10.1130/G24149A.1, 2007.

Aiuppa, A., Giudice, G., Gurrieri, S., Liuzzo, M., Burton, M., Caltabiano, T., McGonigle, A. J. S., Salerno, G., Shinohara, H., and Valenza, M.: Total volatile flux from Mount Etna, Geophys. Res. Lett., 35, L24302, doi:10.1029/2008GL035871, 2008.

Aiuppa, A., Cannata, A., Cannavò, F., Di Grazia, G., Ferrari, F., Giudice, G., Gurrieri, S., Liuzzo, M., Mattia, M., Montalto, P., Patanè, D., and Puglisi, G.: Patterns in the recent 2007–2008 activity of Mount Etna volcano investigated by integrated geophysical and geochemical observations, Geochem. Geophy. Geosy., 11, Q09008, doi:10.1029/2010GC003168, 2010.

Aiuppa, A., Fiorani, L., Santoro, S., Parracino, S., Nuvoli, M., Chiodini, G., Minopoli, C., and Tamburello, G.: New ground-based lidar enables volcanic CO_2 flux measurements, Sci. Rep., 5, 13614, doi:10.1038/srep13614, 2015.

Allard, P., Carbonnelle, J., Dajlevic, D., Bronec, J. L., Morel, P., Robe, M. C., Maurenas, J. M., Faivre-Pierret, R., Martin, D., Sabroux, J. C., and Zettwoog, P.: Eruptive and diffuse emissions of CO_2 from Mount Etna, Nature, 352, 387–391, doi:10.1038/351387a0, 1991.

Bobrowski, N., Hönninger, G., Galle, B., and Platt, U.: Detection of bromine monoxide in a volcanic plume, Nature, 423, 273–276, doi:10.1038/nature01625, 2003.

Burrows, J., Richter, A., Dehn, A., Deters, B., Himmelmann, S., Voigt, S., and Orphal, J.: Atmospheric remote-sensing reference data from GOME – 2. Temperature-dependent absorption cross sections of O_3 in the 231–794 nm range, J. Quant. Spectrosc. Ra., 61, 509–517, doi:10.1016/S0022-4073(98)00037-5, 1999.

Burton, M. R., Oppenheimer, C., Horrocks, L. A., and Francis, P. W.: Remote sensing of CO_2 and H_2O emission rates from Masaya volcano, Nicaragua, Geology, 28, 915–918, doi:10.1130/0091-7613(2000)28<915:RSOCAH>2.0.CO;2, 2000.

Burton, M. R., Sawyer, G. M., and Granieri, D.: Deep Carbon Emissions from Volcanoes, Rev. Mineral. Geochem., 75, 323–354, doi:10.2138/rmg.2013.75.11, 2013.

D'Aleo, R., Bitetto, M., Delle Donne, D., Tamburello, G., Battaglia, A., Coltelli, M., Patanè, D., Prestifilippo, M., Sciotto, M., and Aiuppa, A.: Spatially resolved SO_2 flux emissions from

Mt Etna, Geophys. Res. Lett., 43, doi:10.1002/2016GL069938, GL069938, 2016.

Fleischmann, O. C., Hartmann, M., Burrows, J. P., and Orphal, J.: New ultraviolet absorption cross-sections of BrO at atmospheric temperatures measured by time-windowing Fourier transform spectroscopy, J. Photochem. Photobiol. A, 168, 117–132, doi:10.1016/j.jphotochem.2004.03.026, 2004.

Francis, P., Burton, M. R., and Oppenheimer, C.: Remote measurements of volcanic gas compositions by solar occultation spectroscopy, Nature, 396, 567–570, doi:10.1038/25115, 1998.

Frey, M., Hase, F., Blumenstock, T., Groß, J., Kiel, M., Mengistu Tsidu, G., Schäfer, K., Sha, M. K., and Orphal, J.: Calibration and instrumental line shape characterization of a set of portable FTIR spectrometers for detecting greenhouse gas emissions, Atmos. Meas. Tech., 8, 3047–3057, doi:10.5194/amt-8-3047-2015, 2015.

Gerlach, T. M., McGee, K. A., Elias, T., Sutton, A. J., and Doukas, M. P.: Carbon dioxide emission rate of Kilauea Volcano: Implications for primary magma and the summit reservoir, J. Geophys. Res., 107, 2189, doi:10.1029/2001JB000407, 2002.

Gisi, M., Hase, F., Dohe, S., and Blumenstock, T.: Camtracker: a new camera controlled high precision solar tracker system for FTIR-spectrometers, Atmos. Meas. Tech., 4, 47–54, doi:10.5194/amt-4-47-2011, 2011.

Gisi, M., Hase, F., Dohe, S., Blumenstock, T., Simon, A., and Keens, A.: XCO_2-measurements with a tabletop FTS using solar absorption spectroscopy, Atmos. Meas. Tech., 5, 2969–2980, doi:10.5194/amt-5-2969-2012, 2012.

Goff, F., Love, S. P., Warren, R., Counce, D., Obenholzner, J., Siebe, C., and Schmidt, S. C.: Passive infrared remote sensing evidence for large, intermittent CO_2 emissions at Popocatépetl volcano, Mexico, Chem. Geol., 177, 133–156, doi:10.1016/S0009-2541(00)00387-9, 2001.

Grutter, M., Basaldud, R., Rivera, C., Harig, R., Junkerman, W., Caetano, E., and Delgado-Granados, H.: SO_2 emissions from Popocatépetl volcano: emission rates and plume imaging using optical remote sensing techniques, Atmos. Chem. Phys., 8, 6655–6663, doi:10.5194/acp-8-6655-2008, 2008.

Hase, F., Hannigan, J., Coffey, M., Goldman, A., Höpfner, M., Jones, N., Rinsland, C., and Wood, S.: Intercomparison of retrieval codes used for the analysis of high-resolution, ground-based FTIR measurements , J. Quant. Spectrosc. Ra., 87, 25–52, doi:10.1016/j.jqsrt.2003.12.008, 2004.

Hase, F., Frey, M., Blumenstock, T., Groß, J., Kiel, M., Kohlhepp, R., Mengistu Tsidu, G., Schäfer, K., Sha, M. K., and Orphal, J.: Application of portable FTIR spectrometers for detecting greenhouse gas emissions of the major city Berlin, Atmos. Meas. Tech., 8, 3059–3068, doi:10.5194/amt-8-3059-2015, 2015.

Hermans, C., Vandaele, A., Fally, S., Carleer, M., Colin, R., Coquart, B., Jenouvrier, A., and Merienne, M.-F.: Absorption Cross-section of the Collision-Induced Bands of Oxygen from the UV to the NIR, in: Weakly Interacting Molecular Pairs: Unconventional Absorbers of Radiation in the Atmosphere, edited by: Camy-Peyret, C. and Vigasin, A. A., 193–202, Springer Netherlands, doi:10.1007/978-94-010-0025-3_16, 2003.

Keppel-Aleks, G., Toon, G. C., Wennberg, P. O., and Deutscher, N. M.: Reducing the impact of source brightness fluctuations on spectra obtained by Fourier-transform spectrometry, Appl. Opt., 46, 4774–4779, doi:10.1364/AO.46.004774, 2007.

Kern, C., Sutton, J., Elias, T., Lee, L., Kamibayashi, K., Antolik, L., and Werner, C.: An automated SO_2 camera system for continuous, real-time monitoring of gas emissions from Kilauea Volcano's summit Overlook Crater, J. Volcanol. Geoth. Res., 300, 81–94, doi:10.1016/j.jvolgeores.2014.12.004, 2015.

Klappenbach, F., Bertleff, M., Kostinek, J., Hase, F., Blumenstock, T., Agusti-Panareda, A., Razinger, M., and Butz, A.: Accurate mobile remote sensing of XCO_2 and XCH_4 latitudinal transects from aboard a research vessel Atmos. Meas. Tech., 8, 5023–5038, doi:10.5194/amt-8-5023-2015, 2015.

La Spina, A., Burton, M., and Salerno, G. G.: Unravelling the processes controlling gas emissions from the central and northeast craters of Mt. Etna, J. Volcanol. Geoth. Res., 198, 368–376, doi:10.1016/j.jvolgeores.2010.09.018, 2010.

Lamouroux, J., Tran, H., Laraia, A. L., Gamache, R. R., Rothman, L. S., Gordon, I. E., and Hartmann, J.: Updated database plus software for line-mixing in CO_2 infrared spectra and their test using laboratory spectra in the 1.52.3 µm region, J. Quant. Spectrosc. Ra., 111, 2321–2331, doi:10.1016/j.jqsrt.2010.03.006, 2010.

Love, S. P., Goff, F., Counce, D., Siebe, C., and Delgado, H.: Passive infrared spectroscopy of the eruption plume at Popocatepetl volcano, Mexico, Nature, 396, 563–567, doi:10.1038/25109, 1998.

Meller, R. and Moortgat, G. K.: Temperature dependence of the absorption cross sections of formaldehyde between 223 and 323 K in the wavelength range 225–375 nm, J. Geophys. Res., 105, 7089, doi:10.1029/1999JD901074, 2000.

Mori, T. and Notsu, K.: Remote CO, COS, CO_2, SO_2, HCl detection and temperature estimation of volcanic gas, Geophys. Res. Lett., 24, 2047–2050, doi:10.1029/97GL52058, 1997.

Mori, T., Notsu, K., Tohjima, Y., and Wakita, H.: Remote detection of HCl and SO_2 in volcanic gas from Unzen Volcano, Japan, Geophys. Res. Lett., 20, 1355–1358, doi:10.1029/93GL01065, 1993.

Naughton, J. J., Derby, J. V., and Glover, R. B.: Infrared measurements on volcanic gas and fume: Kilauea eruption, 1968, J. Geophys. Res., 74, 3273–3277, doi:10.1029/JB074i012p03273, 1969.

Norton, R. H. and Beer, R.: New apodizing functions for Fourier spectrometry: errata, J. Opt. Soc. Am., 67, 419–419, 1977.

Platt, U. and Stutz, J.: Differential Optical Absorption Spectroscopy (DOAS), Principle and Applications, ISBN 978-3-540-75776-4, Springer Verlag, Heidelberg, 2008.

Rothman, L. S., Gordon, I. E., Barbe, A., Benner, D. C., Bernath, P. F., Birk, M., Boudon, V., Brown, L. R., Campargue, A., Champion, J., Chance, K., Coudert, L. H., Dana, V., Devi, V. M., Fally, S., Flaud, J., Gamache, R. R., Goldman, A., Jacquemart, D., Kleiner, I., Lacome, N., Lafferty, W. J., Mandin, J., Massie, S. T., Mikhailenko, S. N., Miller, C. E., Moazzen-Ahmadi, N., Naumenko, O. V., Nikitin, A. V., Orphal, J., Perevalov, V. I., Perrin, A., Predoi-Cross, A., Rinsland, C. P., Rotger, M., Šimečková, M., Smith, M. A. H., Sung, K., Tashkun, S. A., Tennyson, J., Toth, R. A., Vandaele, A. C., and Vander Auwera, J.: The HITRAN 2008 molecular spectroscopic database, J. Quant. Spectrosc. Ra., 110, 533–572, doi:10.1016/j.jqsrt.2009.02.013, 2009.

Salerno, G., Burton, M., Oppenheimer, C., Caltabiano, T., Randazzo, D., Bruno, N., and Longo, V.: Three-years of {SO_2} flux measurements of Mt. Etna using an automated {UV} scanner array: Comparison with conventional traverses and uncer-

tainties in flux retrieval, J. Volcanol. Geoth. Res., 183, 76–83, doi:10.1016/j.jvolgeores.2009.02.013, 2009.

Shinohara, H., Aiuppa, A., Giudice, G., Gurrieri, S., and Liuzzo, M.: Variation of H_2O / CO_2 and CO_2 / SO_2 ratios of volcanic gases discharged by continuous degassing of Mount Etna volcano, Italy, J. Geophys. Res., 113, B09203, doi:10.1029/2007JB005185, 2008.

Stremme, W., Ortega, I., Siebe, C., and Grutter, M.: Gas composition of Popocatépetl Volcano between 2007 and 2008: FTIR spectroscopic measurements of an explosive event and during quiescent degassing, Earth Planet. Sc. Lett., 301, 502–510, doi:10.1016/j.epsl.2010.11.032, 2011.

Stremme, W., Krueger, A., Harig, R., and Grutter, M.: Volcanic SO_2 and SiF4 visualization using 2-D thermal emission spectroscopy – Part 1: Slant-columns and their ratios, Atmos. Meas. Tech., 5, 275–288, doi:10.5194/amt-5-275-2012, 2012.

Theys, N., Campion, R., Clarisse, L., Brenot, H., van Gent, J., Dils, B., Corradini, S., Merucci, L., Coheur, P.-F., Van Roozendael, M., Hurtmans, D., Clerbaux, C., Tait, S., and Ferrucci, F.: Volcanic SO_2 fluxes derived from satellite data: a survey using OMI, GOME-2, IASI and MODIS, Atmos. Chem. Phys., 13, 5945–5968, doi:10.5194/acp-13-5945-2013, 2013.

Toon, G. C.: Telluric line list for GGG2014, doi:10.14291/tccon.ggg2014.atm.R0/1221656, 2014.

Vandaele, A., Hermans, C., Simon, P., Carleer, M., Colin, R., Fally, S., Mérienne, M., Jenouvrier, A., and Coquart, B.: Measurements of the NO_2 absorption cross-section from 42 000 cm^{-1} to 10 000 cm^{-1} (238–1000 nm) at 220 K and 294 K, J. Quant. Spectrosc. Ra., 59, 171–184, doi:10.1016/S0022-4073(97)00168-4, 1998.

Vandaele, A., Hermans, C., and Fally, S.: Fourier transform measurements of SO_2 absorption cross sections: II., J. Quant. Spectrosc. Ra., 110, 2115–2126, doi:10.1016/j.jqsrt.2009.05.006, 2009.

Voigt, C., Jessberger, P., Jurkat, T., Kaufmann, S., Baumann, R., Schlager, H., Bobrowski, N., Giuffrida, G., and Salerno, G.: Evolution of CO_2, SO_2, HCl, and HNO_3 in the volcanic plumes from Etna, Geophys. Res. Lett., 41, 2196–2203, doi:10.1002/2013GL058974, 2014.

Wunch, D., Toon, G. C., Wennberg, P. O., Wofsy, S. C., Stephens, B. B., Fischer, M. L., Uchino, O., Abshire, J. B., Bernath, P., Biraud, S. C., Blavier, J.-F. L., Boone, C., Bowman, K. P., Browell, E. V., Campos, T., Connor, B. J., Daube, B. C., Deutscher, N. M., Diao, M., Elkins, J. W., Gerbig, C., Gottlieb, E., Griffith, D. W. T., Hurst, D. F., Jiménez, R., Keppel-Aleks, G., Kort, E. A., Macatangay, R., Machida, T., Matsueda, H., Moore, F., Morino, I., Park, S., Robinson, J., Roehl, C. M., Sawa, Y., Sherlock, V., Sweeney, C., Tanaka, T., and Zondlo, M. A.: Calibration of the Total Carbon Column Observing Network using aircraft profile data, Atmos. Meas. Tech., 3, 1351–1362, doi:10.5194/amt-3-1351-2010, 2010.